Polarization-dependent frequency shifts from Rb-^{3}He collisions

N. R. Newbury, A. S. Barton, P. Bogorad, G. D. Cates, M. Gatzke, H. Mabuchi, and B. Saam
Physics Department, Princeton University, Princeton, New Jersey 08544
(Received 3 August 1992)

We present measurements of the frequency shift of the Rb electron-paramgnetic-resonance (EPR) line in the presence of nuclear-polarized ^{3}He gas for the temperature range of 30 to 85 °C. The frequency shift is due to the Fermi-contact interaction between the Rb valence electron and the polarized ^{3}He nucleus. Expressions for both the frequency shift and the spin-exchange cross section are derived in terms of the strength of this contact interaction. From these expressions and the measured frequency shift, we estimate the Rb-^{3}He spin-exchange cross section. The Rb EPR frequency shift, which is 53 kHz for a 100% polarized 10-amagat ^{3}He sample at 50 °C, can be used to determine the absolute polarization of nuclear polarized ^{3}He targets. From these measurements, one can also predict the shift of the ^{3}He NMR line due to a polarized Rb vapor.

PACS number(s): 32.80.Bx, 32.30.Dx, 33.25.−j, 33.35.−q

I. INTRODUCTION

Noble gases with nonzero nuclear spin can be polarized through spin exchange with optically pumped alkali-metal atoms [1–5]. A wide variety of experiments in atomic [6, 7], nuclear [8–10], and particle physics [11] have employed this method to polarize ^{3}He. Many of these experiments have required absolute calibration of the ^{3}He polarization. As pointed out by Schaefer *et al.* [12], a promising form of noble-gas polarimetry uses the frequency shift of the alkali-metal electron-paramagnetic-resonance (EPR) line due to the effective magnetic field produced by a polarized noble gas. In this work we present an experimental measurement of the EPR frequency shift of Rb due to nuclear-polarized ^{3}He gas in which the polarization is well calibrated. Our results have already been used to determine the ^{3}He target polarization in a recent study of muonic He [6].

Spin exchange between the spin $\mathbf{S}$ of an alkali-metal-atom valence electron and the nuclear spin $\mathbf{K}$ of a noble-gas atom results from the Fermi-contact interaction $\alpha\mathbf{K}\cdot\mathbf{S}$. This interaction also produces a shift in the EPR frequency of the alkali-metal atom if the noble gas is polarized and a shift in the nuclear-magnetic-resonance (NMR) frequency of the noble-gas atom if the alkali-metal vapor is polarized [3, 12]. As pointed out by Grover [13] these shifts are larger than one would expect classically. Following Schaefer *et al.* [12], we characterize this enhancement by the dimensionless factors κ_{AX} and κ_{XA}. The shift in the frequency of the alkali-metal EPR line is then [12]

$$\Delta|\nu_A| = \frac{1}{h}\frac{\mu_B|g_s|}{2I+1}\kappa_{AX}\frac{8\pi}{3}\mu_K\frac{\langle K_z\rangle}{K}[X], \tag{1}$$

where I is the nuclear spin of the relevant alkali-metal isotope, $g_s \approx 2$ is the electron g factor, h is Planck's constant, μ_B is the Bohr magneton, $[X]$ is the number density of noble-gas atoms, and μ_K is the noble-gas nuclear magnetic moment. Similarly the shift in the frequency of the NMR line is

$$\Delta|\nu_X| = \frac{-|\mu_K|}{hK}\kappa_{XA}\frac{8\pi}{3}g_s\mu_B\langle S_z\rangle[A], \tag{2}$$

where $[A]$ is the alkali-atom number density. In general, κ_{AX} and κ_{XA} have a contribution both from bound alkali-metal–noble-gas van der Waals molecules and from free alkali-metal–noble-gas pairs. For helium, binary collisions completely dominate and the two enhancement factors are equal. In keeping with the notation of Schaefer *et al.*, we write $\kappa_{AX} = \kappa_{XA} = \kappa_0$. The enhancement factor κ_0 is defined such that at high enough pressures for all alkali-metal–noble-gas pairs both κ_{AX} and κ_{XA} will approach the common limiting value of κ_0 [12].

Although the spin-exchange cross section has been experimentally determined for many alkali-metal–noble-gas pairs, the enhancement factor κ_0 has been determined only for the Rb-Xe and the Rb-Kr systems [12]. We have made absolute measurements of κ_0 for the Rb-^{3}He system using two completely independent experimental techniques. The two experiments were performed at different temperatures, 55 and 85 °C. In addition, in part to facilitate the comparison of these two experiments, we have separately measured the temperature dependence of κ_0 from 30 to 85 °C. As expected [12], κ_0 is linear in the temperature,

$$\kappa_0(T) = \kappa_0(100\,^\circ\mathrm{C})\left(1+\frac{T-(100\,^\circ\mathrm{C})}{T_0}\right). \tag{3}$$

From our measurements, we find $\kappa_0(100\,^\circ\mathrm{C}) = 5.17\pm0.37$ and $T_0 = 563\pm30\,^\circ\mathrm{C}$. We have chosen the reference temperature of 100 °C to facilitate comparison with Walker's calculations [14]. This value of κ_0 yields a shift (1) in the EPR line of ^{85}Rb at 50 °C of 53.1 ± 3.8 kHz assuming a ^{3}He density of 10 amagats and a polarization of 100%. (An amagat is a unit of density corresponding to 1 atm at 0 °C.)

The contact interaction responsible both for spin exchange and frequency shifts is very much smaller than

the alkali-metal–noble-gas interatomic potential. We can therefore derive essentially exact quantum-mechanical expressions for both σ_{SE} and κ_0 from perturbation theory in terms of the matrix elements of $\alpha(r)$ between the radial eigenfunctions of the interatomic potential. In the semiclassical limit, these expressions reduce to those used by Walker to calculate κ_0 and σ_{SE} for all alkali-metal–noble-gas pairs [14]. Walker's calculations are based on a theoretical derivation [15] of the coupling strength $\alpha(r)$ as a function of the internuclear separation r. For alkali-metal–He collisions there is a theoretical uncertainty of about a factor of 2 in the absolute strength of $\alpha(r)$ and a corresponding uncertainty in Walker's predictions. We show, however, that the ratio of Walker's values for κ_0^2 and σ_{SE} should be largely free of uncertainties in $\alpha(r)$ and depends only on the interatomic potential and the validity of the semiclassical approximation. We can therefore estimate the spin-exchange cross section from our value of κ_0 in the hopes of resolving an existing discrepancy of about a factor of 2 in the published values of the velocity-averaged spin-exchange cross section $\langle \sigma_{SE} v \rangle$ [5, 16, 17].

There are of course additional shifts to the alkali-metal EPR frequency. Some well-studied phenomena are light shifts [18], alkali-metal–alkali-metal spin-exchange shifts [19, 20], the Bloch-Siegert shift [21], and magnetic-field inhomogeneity shifts [22]. These shifts are typically only a few hertz, much smaller than the $\sim$ 20 kHz shifts described in this paper. Potentially the most important additional shift is due to the long-range dipole-dipole interaction. The frequency shift of an alkali-metal atom caused by the surrounding polarized gas has both a short-range contribution given by (1) and a long-range contribution which can be determined classically. To calculate the total EPR frequency shift, it is useful to consider a small sphere around the alkali-metal atom. The frequency shift caused by the polarized noble gas within the sphere is given by (1), where κ_0 must be calculated quantum mechanically. The additional frequency shift caused by the polarized noble gas outside the sphere is simply proportional to the classical macroscopic magnetic field produced by these spins at the location of the alkali-metal atom. This classical macroscopic magnetic field depends on the shape of the sample and vanishes in the case of a sphere. The cells used in the experiments described here were sufficiently spherical that the shift was completely dominated by (1). However, for a cylindrical cell filled with polarized ^{3}He, the long-range contribution to the Rb EPR frequency shift can be as much as 10% of the short-range contribution (1).

II. EXPERIMENTAL MEASUREMENTS OF κ_0

The experiments to determine κ_0 were all performed using spherical glass cells with diameters of $\sim$2.5 cm containing about 100 Torr of N_2, a few milligrams of natural Rb and $\sim$ 8 amagat of ^{3}He (Table I). The exact procedures used to produce the cells can be found in more detail elsewhere [23].

The volumes of the cells were determined by applying Archimedes' principle. The cells were floated in water within a nylon bag. Sufficient weights were hung from the bag such that the buoyancy force and the combined weight of the cell and weights were perfectly balanced. The known density of the weights, aluminosilicate glass (Corning No. 1720), and nylon allowed us to determine the cell volume to 1%.

TABLE I. Properties of the aluminosilicate glass cells used in these experiments. All cells are very nearly spherical except for small protruding stems, and contain 80–110 Torr N_2. Cell 1 was used in the water-calibrated experiment, cell 3 in the far-field calibrated experiment, and cell 2 in the temperature-dependence studies.

Cell No.	$[^3\mathrm{He}]$ (amagat)	V (cm^{-3})
1	7.69 ± 0.19	7.71 ± 0.08
2	7.21 ± 0.18	6.81 ± 0.07
3	8.37 ± 0.20	5.84 ± 0.06

The cells were first heated to 175–200 °C to achieve Rb number densities of 10^{14}– 10^{15} cm^{-3}. A 5-W Ti:sapphire laser optically pumped the Rb atoms at the D_1 line (795 nm). Over a period of hours, the ^{3}He nuclei became polarized to 10–50 % by spin-exchange collisions with the polarized Rb vapor [5]. After polarizing the sample, the laser beam was blocked and the cell was cooled to 55–85 °C. At these temperatures most of the Rb condenses on the walls and the ^{3}He nuclear relaxation was dominated by magnetic-field inhomogeneities [22], paramagnetic impurities on the walls and in the gas, and by bulk dipole-dipole relaxation [23].

We have performed two absolute measurements of κ_0. In both experiments, the value of κ_0 was determined from (1) by measuring of the frequency shift of the ^{85}Rb EPR line isotope while simultaneously measuring the ^{3}He polarization. The method of measuring the ^{3}He polarization differed between the two experiments. In the first experiment, an adiabatic-fast-passage (AFP) NMR signal from the ^{3}He was compared to the AFP signal of water held at a known temperature and magnetic field. In the second experiment, the external macroscopic magnetic field of the polarized ^{3}He cell was measured with an optically pumped ^{133}Cs magnetometer [24–26]. The magnetization, and hence the ^{3}He polarization, was calculated from the macroscopic field using classical electromagnetism. Finally, the temperature dependence of κ_0 was determined by measuring the frequency shift of a polarized cell as a function of temperature.

A. Determining the Rb EPR frequency

Common to all the measurements described in this paper was a system shown schematically in Fig. 1, which locks a voltage-controlled oscillator (VCO) to the Rb EPR frequency [24–26]. The apparatus was similar to that of Schaefer *et al.* [12], except that the nominal magnetic field of 1 G was a factor of 10 higher than was used by Schaefer *et al.* and was supplied by a pair of Helmholtz coils instead of a shielded solenoid. Circularly polarized 795-nm D_1 light from a Rb resonance lamp propagated along the magnetic-field axis and optically pumped the

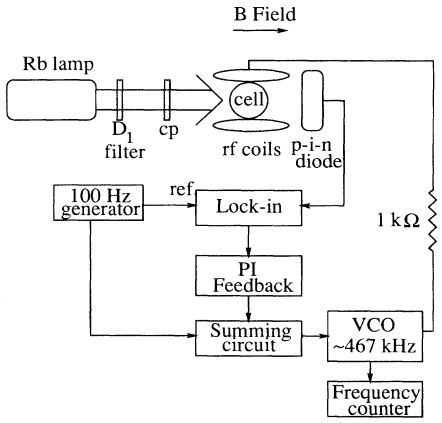

FIG. 1. Schematic of the apparatus used to lock the Rb EPR frequency in the experiments described in Secs. II B, II C, and II D. The proportional-integral (PI) feedback circuit keeps the VCO locked to the ^{85}Rb EPR frequency. A similar setup was used with a ^{133}Cs cell to lock the main magnetic field to 1 G, except that the output of the PI feedback circuit was sent to the input of the current supply for the Helmholtz coils. Device CP circularly polarizes the light.

alkali-metal vapor. An oscillating rf field of the form $H_1 \cos(2\pi\nu t + \Delta\phi \sin 2\pi\nu_m t)$ was applied perpendicular to the axis of the light. Typically the modulation frequency $\nu_m \approx 100$ Hz and the magnitude of the phase modulation $\Delta\phi \approx 3\pi$. As described below, the central rf frequency ν was locked to the Larmor frequency ν_0 of ^{85}Rb, which was near 467 kHz depending on the exact value of the applied main magnetic field and the effective field of the ^{3}He nuclear spins. The transmitted D_1 pump light was focused onto a *p-i-n* diode, the output of which was referenced to ν_m using a lock-in amplifier. In the limit of low-frequency modulation, the Fourier component of the transmission signal at ν_m is proportional to the derivative of the EPR line shape and is thus zero for a detuning $\Delta\nu = \nu - \nu_0 = 0$. For a small value of $\Delta\nu$, this signal is linear in $\Delta\nu$ and provides an error signal in a feedback loop to lock ν to the Zeeman splitting ν_0 (Fig. 1). The locked rf frequency ν was averaged over a 10-sec interval by a frequency counter, and the result was recorded by a personal computer.

Since linear rather than circularly polarized rf was applied, the Zeeman resonances within both the hyperfine multiplets ($F = 3$ and $F = 2$) were observed. At 1 G, the nuclear magnetic moment splits the Zeeman resonances of the $F = 3$ and $F = 2$ hyperfine multiplets by about 0.8 kHz. The small quadratic dependence of the Zeeman energy levels on the magnetic-field further broadens the resonance by about 0.8 kHz. The broadening from magnetic-field inhomogeneities was 2–4 kHz. Sufficient rf was applied to the cell to power broaden the resonance line to a full width at half maximum (FWHM) of about 8 kHz.

An actual measurement of κ_0 took a number of hours, so it was important that the main magnetic field be stable to ~ 100 μG or less. The main magnetic field was locked using a similar technique to that described above with a ^{133}Cs magnetometer placed about 10 cm from the Rb-^{3}He cell. (In order to lock the field, the error signal from the Cs cell was sent to the input of the bipolar operational amplifier which supplies the current for the main magnetic field.) The main systematic error in the frequency-shift measurement was due to changing magnetic-field gradients between the Cs magnetometer and the Rb cell, which led to variations in the baseline of the Rb EPR frequency (i.e., the Rb EPR frequency in the absence of ^{3}He polarization). These baseline variations were typically only 50–100 Hz. The stability of the baseline frequency was monitored in two ways. First, it was possible to remove the polarized cell and insert an unpolarized cell in the same position to determine the baseline at any time. Second, the frequency shift was usually taken as the difference between the Rb EPR frequency as measured with the ^{3}He polarization parallel and antiparallel to the main magnetic field. Other possibly important systematic shifts in the Rb EPR line were due to changes in the magnitude of the pumping light, the applied rf field, and the frequency modulation. These other effects caused shifts well below 50 Hz. The error in determining the frequency shifts was typically less than 1–4%, depending on the size of the shift. The error in measuring κ_0 was thus dominated by the larger errors in calibrating the ^{3}He polarization.

B. Water-calibrated experiment

The standard method of calibrating the polarization of a ^{3}He target has been through the adiabatic-fast-passage (AFP) NMR signal [5, 17]. To perform the AFP, a constant rf field is applied perpendicular to the main magnetic field, while the main field is swept through the Larmor resonance of the nuclear spins [27]. If the magnetic field is swept slowly enough to be adiabatic, yet fast enough to avoid losses due to magnetic-field inhomogeneities, the nuclear magnetization of the entire sample will reverse its direction relative to the main field. A set of pick-up coils, perpendicular to both the rf drive coils and the main field, can be used to detect the precessing magnetization as it reverses direction. Provided sufficient rf is applied to power broaden the line, the signal height S from the pick-up coils will be given by

$$S = G\left[[\mathrm{He}]V\mu_{\mathrm{He}}\frac{\langle K_z\rangle}{K}\right], \tag{4}$$

where G is the gain of the pick-up circuit at the rf frequency in units of $(\mathrm{V\,cm^{-3}\,G^{-1}})$, V is the cell volume, and the quantity in large brackets is the total magnetic moment of the polarized ^{3}He. To determine S we fit the AFP signal to the known power-broadened line shape [5, 27].

The AFP system we used resembles that of Coulter [28] and Chupp *et al.* [5], except that it operated at a much higher rf frequency of 2.2 MHz, with the corresponding ^{3}He NMR at 676 G and the water NMR at 516 G. At these high fields, the magnetic-field gradients at the cell were ~50 mG/cm. In order to ensure that the ^{3}He AFP signals were power broadened, a rf power amplifier was

used to produce fields with an amplitude of $\sim$ 600 mG. The precessing magnetization was sensed by a pair of 2.5-cm-diam pick-up coils composed of 20 turns of Litz wire. The pick-up coils acted as the inductor of a tank circuit tuned to 2.2 MHz with a $Q \sim 75$. The tank circuit was buffered with a preamplifier, the output of which was canceled by an adder circuit when the field was off resonance. The output of the adder circuit was referenced to 2.2 MHz using a lock-in amplifier. The lock-in was adjusted to be 90° out of phase with the microphonic noise and thus in phase with the signal [27]. The output of the lock-in was recorded by a computer as the field was swept through resonance. A typical ^{3}He AFP signal is shown in Fig. 2.

A measurement of κ_0 consisted of alternate measurements of ^{3}He AFP signals and Rb EPR frequency shifts. After polarizing the ^{3}He, the cell temperature was lowered to 55 °C, and the field was locked to 1 G using a ^{133}Cs magnetometer. The Rb EPR frequency was recorded for 10–30 min as described in Sec. II A. Next, the field was raised to ~680 G, and one, two, or three AFP signals were taken successively. For an odd number of AFP flips, the sign of the ^{3}He polarization, and therefore of the frequency shift, was reversed. The field was then relocked to 1 G and the EPR line of the Rb was again recorded for 10–30 min. After repeating this sequence five times, the cell was depolarized and the Rb EPR frequency was measured to determine a baseline frequency. This baseline frequency agreed with the midpoint between the EPR frequencies measured before and after an odd number of AFP flips. The EPR frequency shift was calculated as the difference between the baseline frequency and the measured EPR frequencies of the polarized cell. Our data are displayed in Fig. 3, which shows the decay of the ^{3}He polarization as monitored separately from both the AFP signal height and the Rb EPR frequency shift.

To calculate a value of κ_0 from these data we combine (1) and (4) to find

$$\kappa_0 = \frac{3GV}{4\gamma_{\mathrm{Rb}}} \left| \frac{\Delta\nu_{\mathrm{Rb}}}{S} \right| , \tag{5}$$

where $\gamma_{\mathrm{Rb}} \equiv g_s\mu_B/[\hbar(2I+1)]$ is the gyromagnetic ratio of Rb. In order to determine the ratio of the initial AFP amplitude S to the corresponding initial frequency shift, $\Delta\nu_{\mathrm{Rb}}$, we fit the data of Figs. 3(a) and 3(b) each to a decaying exponential, finding an average decay time constant of 2040 ± 100 sec. (We note that subsequent to this measurement we developed cell-fabrication techniques giving polarization decay times an order of magnitude longer than this.) The Rb EPR baseline frequency is uncertain to ±100 Hz, contributing a 4% error to $\Delta|\nu_{\mathrm{Rb}}|$. The dominant error in κ_0 comes from the calibration constant G which we discuss next.

The gain G of the AFP system was calibrated by measuring the AFP signal of the protons in a water cell held at 516 G, corresponding to a proton NMR frequency of 2.2 MHz. The AFP water signal height can be related to the known water magnetization similarly to (4). Thus, the gain $G = S_W/M_W$, where S_W is the fitted water AFP signal height and M_{W} is the total magnetization of the water cell at 516 G and 23 °C. A typical AFP water signal is shown in Fig. 4. The signal-to-noise ratio for an individual water AFP signal was 10 or less; however, signal averaging of 10 to 75 water AFP signals reduced the error to $\lesssim$3%. Unfortunately, there was a slow drift of $\sim$ 6% in G over time presumably due to drifts in the Q of the pick-up coil. In Fig. 5 we show several separate measured values of G.

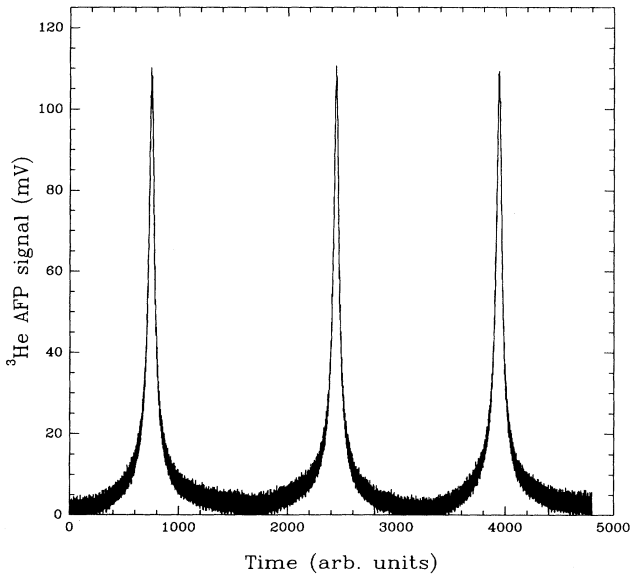

FIG. 2. Three succesive adiabatic-fast-passage signals of a polarized ^{3}He cell. The main magnetic field is ramped linearly through resonance at 16 G/sec. Each sweep through resonance reverses the direction of the ^{3}He polarization with respect to the main magnetic field. The polarization losses in each scan were negligible.

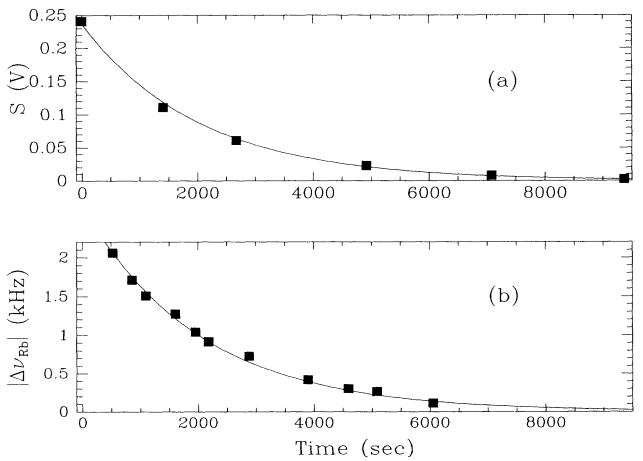

FIG. 3. Decay of ^{3}He polarization as measured (a) by the AFP signal height and (b) by the Rb EPR frequency shift. The solid line in both figures is a decaying exponential with a time constant of 2040 sec, which is the average decay lifetime as measured by the two techniques.

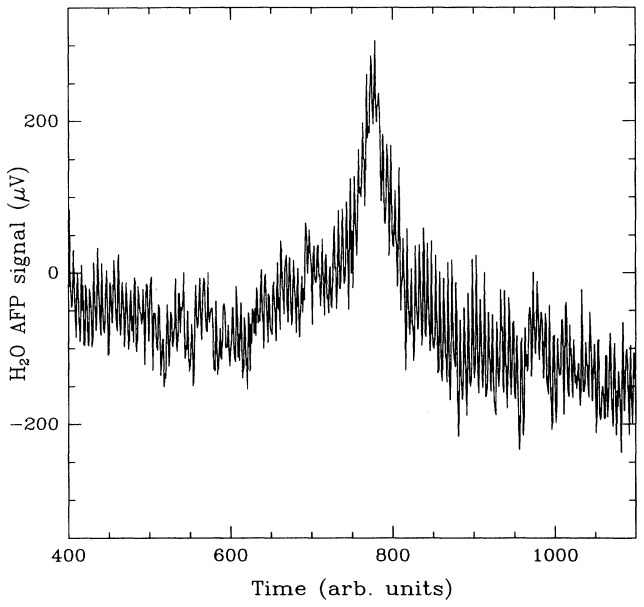

FIG. 4. Adiabatic-fast-passage signal showing the proton resonance in a cell containing deionized water. Note that the small cell volumes and the small Boltzmann polarization limit the signal-to-noise ratio of the water NMR signals.

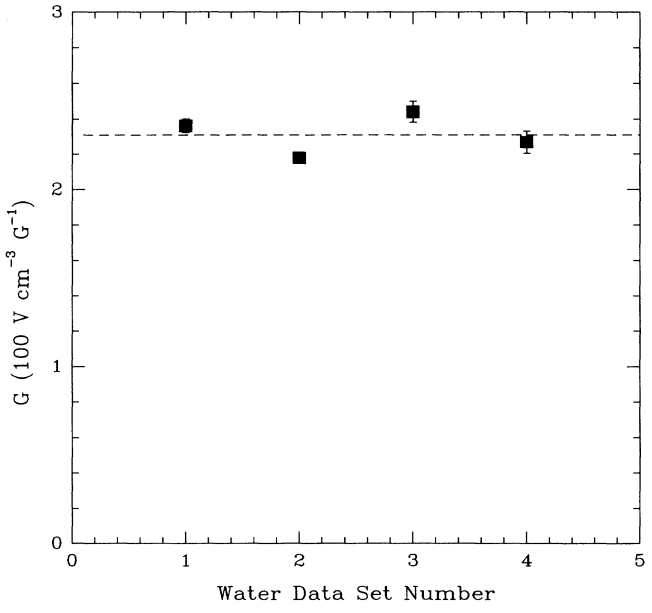

FIG. 5. The AFP system gain G at 55 °C as measured on different days surrounding the κ_0 measurement. Data sets 1–4 represent the average of 44, 75, 10, and 16 water AFP signals, respectively. The errors are the reduced standard deviation of each set of data. The dashed line is the unweighted average of the four data points which gives $G = 231 \pm 17$ V cm^{-3} G^{-1}, where the error represents a conservative estimate of the uncontrolled drifts in the apparatus.

Two corrections were applied to G. First, although the ^{3}He AFP signals were taken with a rf power amplifier, we were unable to use the power amplifier with the water cells because of the resulting large increase in the noise. Studies of the water AFP signal height (at 516 G) versus rf power and of the ^{3}He AFP signal height (at 676 G) taken with and without the power amplifier indicate that the measured AFP water signal height was $98\% \pm 2\%$ of the true power-broadened height. Second, the water AFP data were taken at room temperature, while the ^{3}He AFP signals were taken at a temperature of 55 °C. The gain of the pick-up circuit was proportional to the Q of the tank circuit formed by the coils and an external capacitor. The Q of this circuit is inversely proportional to the pick-up coil resistance, which in turn depends linearly on temperature. Since the pick-up coils were inside the oven, we assume that the gain $G \propto 1/T$. This temperature dependence was confirmed by examining the system response at room temperature, 60 and 180 °C. The temperature correction was $10\% \pm 3\%$. The cell was not completely spherical. A small stem (~ 0.1 cm^{-3}) protruded from one side of the cell. A correction of $2.7 \pm 2\%$ was applied to the value of κ_0 as calculated from (5) due to the effects of this stem on S and $\Delta\nu_{Rb}$. From the water-calibrated experiment, we conclude that $\kappa_0 = 5.11 \pm 0.51$ at 55 °C.

C. Far-field calibrated experiment

In the second experiment, the noble-gas polarization was calibrated by measuring, outside of the cell, the macroscopic magnetic field produced by the polarized ^{3}He gas. Since the polarized cell was spherical, the macroscopic field was dipolar. The component of this field along the main applied magnetic field **B** was sensed by another ^{133}Cs magnetometer system similar to the one used to lock the magnetic field (see Fig. 6). The

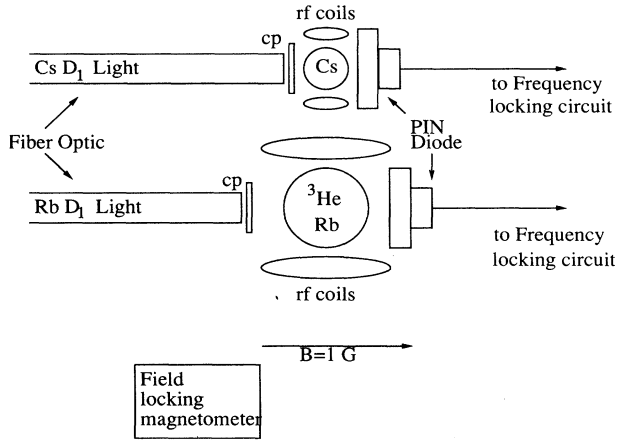

FIG. 6. Schematic of the far-field-calibrated experiment to measure κ_0. The same set of frequency-locking electronics, shown in Fig. 1, were used to measure both the ^{85}Rb and ^{133}Cs EPR frequencies. The Cs and ^{3}He cells were 3.4-cm apart. (A circular polarizer is indicated by CP.)

Cs magnetometer resonance frequency was shifted by an amount

$$\Delta|\nu_{\mathrm{Cs}}| = \frac{\gamma_{\mathrm{Cs}}}{2\pi}[\mathrm{He}]V\mu_{\mathrm{He}}\frac{\langle K_z\rangle}{K}C\,, \tag{6}$$

where γ_{Cs} is the gyromagnetic ratio of ^{133}Cs. The product $\mu_{\mathrm{He}}C$ is the magnetic field due to the ^{3}He nuclei, spatially averaged over the volume of the Cs cell. Since the Cs cell effectively senses only the magnetic field of the ^{3}He parallel to the applied field direction $\hat{z}$,

$$C \equiv \frac{1}{V_{\mathrm{Cs}}}\int_{V_{\mathrm{Cs}}}\frac{3(\hat{\mathbf{r}}\cdot\hat{\mathbf{z}})^2-1}{r^3}d^3r, \tag{7}$$

where $\mathbf{r}$ is a vector pointing from the center of the polarized ^{3}He cell to a point within the Cs cell and the integral is over the volume V_{Cs} of the Cs cell. In writing (7) we assume that the field lines of the applied magnetic field at the locations of the Cs cell and the Rb cell are parallel, a condition easily met in our Helmholtz coils.

The constant κ_0 can be determined from measurements of the Cs EPR frequency shift (6) and the frequency shift (1) of the EPR line of the Rb in the polarized ^{3}He cell. Combining these equations yields

$$\kappa_0 = \frac{3}{8\pi}\frac{\gamma_{\mathrm{Cs}}}{\gamma_{\mathrm{Rb}}}\frac{\Delta|\nu_{\mathrm{Rb}}|}{\Delta|\nu_{\mathrm{Cs}}|}VC\,. \tag{8}$$

To evaluate κ_0 from (8) we determined the frequency ratio $\Delta|\nu_{\mathrm{Rb}}|/\Delta|\nu_{\mathrm{Cs}}|$ and the volume integral C.

A schematic of the setup is shown in Fig. 6. A ^{3}He cell (see Table I) polarized to 30–50 % was held at 85 °C and the Rb EPR frequency was measured using the technique discussed in Sec. II A. The ^{3}He magnetization was reversed by an AFP sweep and the Rb frequency remeasured yielding an initial Rb frequency shift. The Cs EPR frequency was then measured a number of times with intervening reversals of the ^{3}He polarization through AFP. The resulting Cs EPR frequency is shown in Fig. 7. Depending on the relative orientation of the ^{3}He spins with respect to the applied field, the Cs frequency shift (6) can be either positive or negative. Despite the high density and polarization of the ^{3}He cell, the maximum dipole field at the Cs cell was only about 80 μG.

We reversed the ^{3}He magnetization by an AFP sweep of the frequency of the applied rf through the ^{3}He NMR frequency of 3.2 kHz at the constant 1-G field. The decay of the ^{3}He polarization (and consequently of the Cs frequency shift) that is evident in Fig. 7 is due to the 10–15 % losses of the ^{3}He polarization incurred during the AFP flip. The intrinsic lifetime of the ^{3}He polarization in this cell was about 80 h and did not contribute significantly to the decay observed in Fig. 7. These losses were a result of the difficulty of satisfying the conditions necessary for the AFP at 1 G with gradients of a few milligauss per centimeter. Performing AFP at a higher magnetic field would have eliminated losses. However, raising and lowering the magnetic field slightly magnetized nearby material, leading to unacceptable changes in the magnetic-field gradients between the Cs cell and the polarized ^{3}He cell. Time-dependent gradients of only a few milligauss per centimeter are sufficient to cause

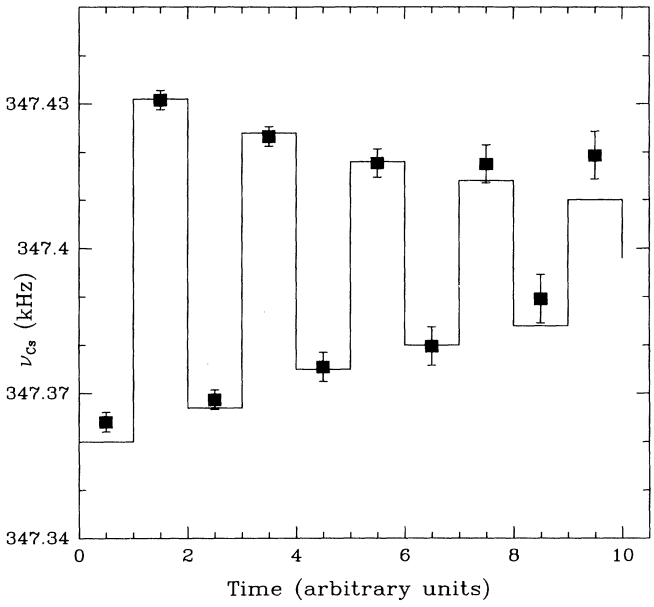

FIG. 7. ^{133}Cs EPR frequency after each reversal of the ^{3}He magnetization by an AFP sweep. Three such runs were performed. In order to analyze the data, the difference in the Cs frequency before and after an AFP flip is used, thereby minimizing the effects of slow drifts in the baseline of about 10 Hz over 30 min. The solid line is a fit to the Cs frequency without accounting for the slow baseline drifts.

significant distortion of the Cs frequency shift.

In order to analyze the data, we define the shift $\Delta\nu_{\mathrm{Rb(Cs)}}(n)$ as the difference in the Rb (Cs) EPR frequency shifts before and after the nth reversal of the ^{3}He magnetization. Ideally, $\Delta\nu_{\mathrm{Rb}}(n)$ should have been measured after every independent measurement of $\Delta\nu_{\mathrm{Cs}}(n)$. This was not possible because of a systematic change on the order of 10 Hz in the measured central resonance frequency associated with disconnecting and reconnecting the locking electronics. Since both the Cs and Rb EPR measurements used the same locking electronics, we adopted the method described above in which only the shifts $\Delta\nu_{\mathrm{Rb}}(1)$, $\Delta\nu_{\mathrm{Rb}}(N)$, and $\Delta\nu_{\mathrm{Cs}}(2)\cdots\Delta\nu_{\mathrm{Cs}}(N-1)$ were measured. The initial frequency shift $\Delta\nu_{\mathrm{Cs}}(1)$ was found by fitting the data to

$$\Delta\nu_{\mathrm{Cs}}(n) = \Delta\nu_{\mathrm{Cs}}(1)X^{n-1}, \tag{9}$$

where $(1-X)$ is the fractional polarization loss from performing AFP. A value for X was determined from the ratio $\Delta\nu_{\mathrm{Rb}}(1)/\Delta\nu_{\mathrm{Rb}}(N)$. To determine the ratio of the frequency shifts appearing in the expression for κ_0 (8) we computed the weighted average of three runs. We found that $\Delta\nu_{\mathrm{Cs}}(1)/\Delta\nu_{\mathrm{Rb}}(1) = 584 \pm 16$.

The dominant error in κ_0 comes from the evaluation of the constant C. The applied magnetic field is the sum of the earth's field and the field produced by a pair of Helmholtz coils. The magnetic-field components were measured precisely using an unpolarized cell as a Rb magnetometer. Numerical integration of (7) over the Cs cell volume of 0.27 cm^{-3} gives $C = 0.0160 \pm 0.0015$ cm^{-3},

where the error is dominated by the uncertainty in the cell-to-cell distance.

Two small corrections were applied to the value of κ_0 calculated from (8). First, the polarized ^{3}He cell was not completely spherical. A small stem protruded from one side of the cell. The effect of the stem on $\Delta\nu_{Cs}(1)$ and $\Delta\nu_{Rb}(1)$ was estimated to reduce κ_0 by $1 \pm 1\%$. Second, the field-locking ^{133}Cs magnetometer (see Sec. II A) will also sense the dipolar field of the polarized cell. Depending on its position, this will result in a slight suppression or enhancement of the measured value of κ_0 over its true value. We have estimated this effect to enhance the measured value of κ_0 by $1.7\% \pm 1.0\%$. From the far-field calibrated experiment, we find a value for κ_0 at 85 °C of 4.75 ± 0.48 from (8).

D. Temperature dependence of κ_0

Following the notation of Schaefer *et al.* [12], Eq. (3) for $\kappa_0(T)$ characterizes the temperature dependence of κ_0 by a temperature coefficient T_0. We have obtained an experimental value for T_0 by measuring the temperature dependence of the Rb EPR frequency shift in a polarized ^{3}He cell. The measurement was performed by locking to the Rb EPR line at 30 °C and then slowly ramping the cell temperature (≤ 3 °C/min) while a computer recorded the EPR locking frequency at regular intervals. After ramping the cell temperature up to 85 °C, we removed the cell to an NMR apparatus where the orientation of the ^{3}He spins relative to the magnetic field was changed from parallel (up) to antiparallel (down) by adiabatic fast passage. The cell was returned to the frequency-shift measurement apparatus. We then recorded the Rb EPR frequency while cooling the cell from 85 °C down to 30 °C. Figure 8 shows the difference in the Rb EPR frequencies as a function of temperature from the spin-up and spin-down runs, corrected for the polarization decay.

Our method was intended to suppress any distortions of the temperature dependence of $\kappa_0(T)$ due to either variations of the baseline Rb frequency with temperature or to the decay of the ^{3}He polarization. We note that the baseline Rb EPR frequency did vary by as much as several hundred Hertz with temperature. However, by considering the difference in the Rb EPR frequency between the spin-up and spin-down runs, we obtained values for the frequency shift which do not depend on systematic variations of the baseline with temperature. The most likely cause of a systematic EPR shift due to temperature changes is changing alkali-metal number densities. For an optically thin vapor, the EPR frequency measured corresponds to the average magnetic field over the cell. However, for an optically thick vapor, the average is weighted toward its value in the front of the cell, where the probe light is incident. In the presence of magnetic-field gradients, this effect can lead to a shift in the EPR frequency.

The ^{3}He polarization lifetime at 1 G was measured to be 52 h and is dominated by the intrinsic bulk relaxation of the ^{3}He [23] and by relaxation due to magnetic-field inhomogeneities [22]. Since the entire measurement lasted only about 2.5 h, we can approximate the polarization decay as linear in time. If the temperature were increased and decreased at the same constant rate, and if there were no polarization losses associated with the AFP polarization reversal, one can easily show that $\kappa_0(T)$ is directly proportional to the measured difference in the spin-up and spin-down Rb EPR frequencies. However, there was a $3\% \pm 1\%$ loss of polarization incurred in reversing the direction of the polarization with respect to the magnetic field. In addition, the rate of change of temperature was not completely constant. The corrections to the data for these effects are straightforward and only a few percent. The frequency shift as a function of temperature shown in Fig. 8 has been corrected for these effects and should therefore be directly proportional to $\kappa_0(T)$.

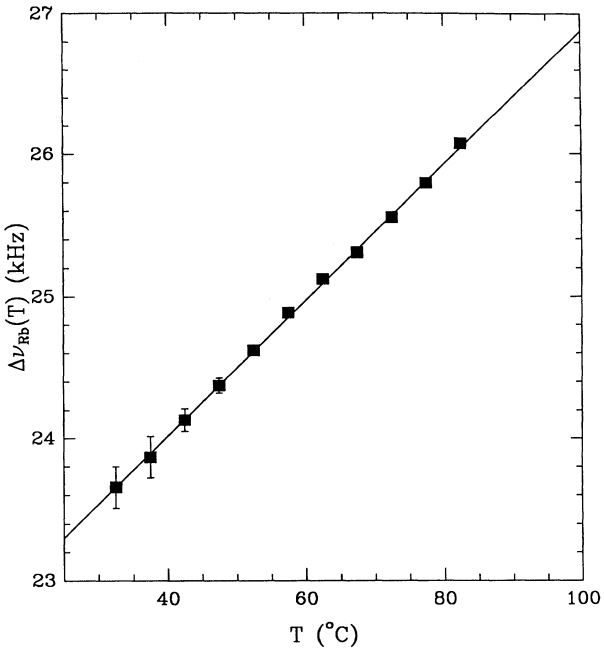

FIG. 8. The temperature dependence of the Rb EPR frequency shift corrected for polarization losses. The corrected frequency shift is proportional to $\kappa_0(T)$, and allows a determination of $T_0 = 563 \pm 30$ °C. The error bars shown are due to the noise in the frequency measurement only.

In order to compare the experimental value of T_0 with the calculated values [12], we use the reference temperature of 100 °C. From the slope of the line in Fig. 8 we find $T_0 = (563 \pm 30)$ °C. As the temperature of the oven is increased, temperature gradients in the oven will also increase. The error in the temperature at 30 °C is estimated to be ±0.2 °C, but at 85 °C the error is as large as ±2.5 °C. The error in T_0 includes the effects of this temperature uncertainty as well as the error in the slope of $\Delta\nu(T)$. The theoretical estimate of Schaefer *et al.* was $T_0 = 440$ °C [12], which, given the approximate nature of their calculation, is consistent with our measured value.

III. THEORY

The interaction between an alkali-metal valence-electron spin and a ^{3}He nuclear spin leads both to spin exchange and frequency shifts of the EPR and NMR lines. Calculation of the spin-exchange cross section σ_{SE} and the enhancement factor κ_{AX} for heavier noble-gas atoms at low pressures is complicated by the formation of long-lived alkali-metal–noble-gas van der Waals molecules. However, the collision time of an alkali-metal atom and a ^{3}He atom of $\sim$1 ps is sufficiently short that we can ignore the hyperfine and Zeeman interactions during the collision. (Clearly for very low temperatures and high magnetic fields this will not always be true.) In this case, alkali-metal–^{3}He spin exchange becomes formally identical in many respects to alkali-metal–alkali-metal, H–H, or electron–alkali-metal spin exchange, in which the same approximation is usually valid. However, for alkali-metal–alkali-metal spin exchange the spin interaction is comparable in magnitude to the interatomic potential, while for alkali-metal–noble-gas spin exchange the spin interaction is the much smaller Fermi contact interaction. Indeed, the Fermi-contact interaction for Rb-^{3}He collisions is typically about ten orders of magnitude smaller than the interatomic potential. Therefore, we can derive essentially exact quantum-mechanical expressions for the velocity-averaged spin-exchange cross section $\langle\sigma_{SE}v\rangle$ and the frequency-shift enhancement factor $\langle\kappa_0\rangle$ based on the distorted-wave Born approximation (DWBA) and the many previous theoretical treatments of alkali-metal–alkali-metal spin exchange [29]. (In this section we will use angle brackets around $\sigma_{SE}v$ and κ_0 to indicate an average over the Boltzmann distribution; the symbols κ_0 and σ_{SE} alone indicate that the quantities are evaluated at definite relative momentum.) We will show that our expressions reduce in the semiclassical limit to those used by Walker [14] in his estimates of $\langle\sigma_{SE}\rangle$ and $\langle\kappa_0\rangle$ for alkali-metal–noble-gas pairs.

A. Derivation of $\langle\sigma_{SE}v\rangle$ and $\langle\kappa_0\rangle$

The Fermi-contact interaction between the alkali-metal-atom valence-electron spin $\mathbf{S}$ and the ^{3}He nuclear spin $\mathbf{K}$ is

$$V'(r) = \alpha(r)\mathbf{K}\cdot\mathbf{S}. \tag{10}$$

If $|\psi(r)|^2$ is the probability per unit volume of finding the alkali-metal valence electron at the noble-gas nucleus for an interatomic separation r, then the coupling constant is

$$\alpha(r) = \frac{8\pi}{3} g_s \mu_B \frac{\mu_K}{K} |\psi(r)|^2 \ . \tag{11}$$

Herman [30] defined an enhancement factor η such that

$$\psi(r) = \eta\phi(r), \tag{12}$$

where $\phi(r)$ is the unperturbed alkali-metal valence-electron wave function, which falls off exponentially with r far outside the alkali-metal atom. The factor η is independent of r to a very good approximation. Walker, Bonin, and Happer [15] have calculated η for ^{3}He using both partial-wave (PW) and orthogonal-plane-wave (OPW) techniques finding $\eta = -5.3$ and $\eta = -9.5$, respectively. We will assume that the collision time is sufficiently long that we can treat (10) in the Born-Oppenheimer approximation as an added spin-dependent interatomic potential.

We will approximate the Hamiltonian for the ^{3}He atom and the alkali-metal atom during a collision as

$$H = H_0 + V'(r) \tag{13}$$

in the center-of-mass system. The unperturbed Hamiltonian is

$$H_0 = \frac{\hbar^2 k^2}{2m} + V_0(r), \tag{14}$$

where m is the reduced mass, $\hbar k$ is the relative momentum, and $V_0(r)$ is the interatomic potential. The perturbing spin-dependent potential (10) can be rewritten in terms of the total spin $\mathbf{F} = \mathbf{K} + \mathbf{S}$ as

$$V'(r) = \frac{\alpha(r)}{2}[F(F+1) - \tfrac{3}{2}] \ , \tag{15}$$

where we have used $K = S = 1/2$. The triplet, $F = 1$, and singlet, $F = 0$, states will suffer different partial-wave phase shifts, δ_l^3 and δ_l^1, respectively, during a collision. This difference in phase shifts causes both the frequency shifts described by (1) and (2) and the spin exchange between the Rb electron spin and the ^{3}He nuclear spin. We define the spin-exchange cross section such that [3]

$$\frac{d}{dt}\langle K_z\rangle = 2[\mathrm{Rb}]\langle\sigma_{SE}v\rangle\big(\langle K(K+1) - K_z^2\rangle\langle S_z\rangle - \langle S(S+1) - S_z^2\rangle\langle K_z\rangle\big). \tag{16}$$

This definition of the velocity-averaged cross section is a factor of 2 larger than the standard definition for alkali-metal–alkali-metal spin exchange, but is consistent with most of the literature on alkali-metal–noble-gas spin exchange. (In alkali-metal–alkali-metal spin exchange one is usually interested in the cross section for spin flips, as opposed to the cross section for the buildup of polarization.) Therefore we include an extra factor of 2 in the expressions for the spin-exchange cross section derived in [20, 31–34] to find

$$\sigma_{SE} = \frac{2\pi}{k^2}\sum_l (2l+1)\sin^2(\delta_l^3 - \delta_l^1) \ , \tag{17}$$

where $l = 0$ to ∞ is the angular-momentum quantum number of the partial wave. The frequency-shift enhancement factor, as defined in (1) is [20, 33]

$$\kappa_0 = \frac{-3\hbar^2}{32\mu_B\mu_K m}\frac{1}{k}\sum_l (2l+1)\sin[2(\delta_l^3 - \delta_l^1)] \ , \tag{18}$$

where we have used $K = 1/2$ and $g_s = 2$. Recoupling of the alkali-metal nuclear spin and the alkali-metal electron spin in between collisions leads to the inclusion of the factor $(2I+1)$ appearing in the denominator of (1).

The impetus of Refs. [20, 31–34] for deriving (17) and

(18) was to understand alkali-metal–alkali-metal, H–H, and electron–alkali-metal spin exchange. If the spin-exchange interaction is between the valence electrons of two atoms, the spatial wave functions of the valence electrons will depend on whether the electrons are in a singlet or triplet state. As a result, the interaction potential for a singlet state is very different from that for a triplet state, and the phase difference $(\delta_l^3 - \delta_l^1)$ is large. In the case of an alkali-metal valence spin interacting with the nuclear spin of a noble-gas atom, the difference in the triplet and singlet potentials is simply the Fermi-contact interaction and is smaller than the interatomic potential by many orders of magnitude. Therefore, the difference in the phase shifts, $\phi_l \equiv \delta_l^3 - \delta_l^1$ can be evaluated essentially exactly in the distorted-wave Born approximation (DWBA).

The radial Schrödinger equation for the unperturbed Hamiltonian (14) is

$$\left(-\partial_r^2 + \frac{2m}{\hbar^2}V_0(r) + \frac{l(l+1)}{r^2} - k^2\right) u_l(r) = 0, \quad (19)$$

where the radial wave functions are chosen to satisfy the boundary conditions

$$u_l(r) \to \begin{cases} 0 \text{ as } r \to 0 & (20) \\ \sin\left(kr - \frac{l\pi}{2} + \delta_l\right) \quad \text{as} \to \infty, & (21) \end{cases}$$

where δ_l is the phase shift due to the spin-independent interatomic potential $V_0(r)$. We assume that the $u_l(r)$ are known, or at least can be found by numerical integration of (19). According to the DWBA, the difference in the phase shifts between the singlet and triplet states is [35, 36]

$$\phi_l = \frac{-2m}{\hbar^2 k}\int_0^\infty u_l^2(r)\alpha(r)dr \equiv \frac{-2m}{\hbar^2 k}\langle\alpha(r)\rangle_l\,, \quad (22)$$

where we have introduced the matrix element of $\alpha(r)$ between the radial eigenfunctions.

The experimentally accessible quantities are the thermal averages of $\sigma_{\rm SE}v$ and κ_0. Keeping only terms to first order in the phase difference and averaging (18) and (17) over a Boltzmann distribution of momenta gives

$$\langle\sigma_{\rm SE}v\rangle = 32\pi^2 m \frac{1}{(2\pi m\kappa T)^{3/2}} \times \int_0^\infty \frac{1}{k}\sum_l (2l+1)\langle\alpha(r)\rangle_l^2\, e^{-\hbar^2k^2/2m\kappa T}dk\,, \quad (23)$$

$$\langle\kappa_0\rangle = \frac{3\pi\hbar^3}{2\mu_B\mu_K}\frac{1}{(2\pi m\kappa T)^{3/2}} \times \int_0^\infty \sum_l (2l+1)\langle\alpha(r)\rangle_l\, e^{-\hbar^2k^2/2m\kappa T}dk\,, \quad (24)$$

where T is temperature and κ is Boltzmann's constant. These expressions could be numerically evaluated by first finding the $u_l(r)$ using the Rb-^{3}He interaction potential of Pascale [37], and then evaluating the matrix elements (22). However, given the large theoretical uncertainty in η, the semiclassical approximation of Walker (Sec. III C) is sufficient [14]. As discussed in more detail below, it may be worthwhile to numerically evaluate the ratio of $\langle\sigma_{\rm SE}v\rangle$ to $\langle\kappa_0\rangle^2$ in order to estimate $\langle\sigma_{\rm SE}v\rangle$ from $\langle\kappa_0\rangle$.

B. Approximate temperature dependence

We can gain some insight into the behavior of these quantities with temperature by the following standard approximation. Since the interaction is short range, the matrix elements $\langle\alpha(r)\rangle_l$ will drop rapidly to zero for angular momenta greater than $l_0 \approx kr_0$, where r_0 is the classical turning point for the $l = 0$ trajectory. Moreover, the matrix element for any partial wave of $l \ll l_0$ will be fairly independent of l and k. Therefore we make the crude approximation that

$$\sum_l (2l+1)\langle\alpha(r)\rangle_l^2 \approx \langle\alpha(r)\rangle_0^2 k^2 r_0^2\,, \quad (25)$$

$$\sum_l (2l+1)\langle\alpha(r)\rangle_l \approx \langle\alpha(r)\rangle_0 k^2 r_0^2\,. \quad (26)$$

Using this approximation in (23) and (24), and assuming that $\langle\alpha(r)\rangle_0$ is independent of k, we find

$$\langle\sigma_{\rm SE}v\rangle = \frac{8}{\hbar^2}\sqrt{\frac{m}{2\pi\kappa T}}\langle\alpha(r)\rangle_0^2(\pi r_0^2), \quad (27)$$

$$\langle\kappa_0\rangle = \frac{3}{8\pi\mu_B\mu_K}\langle\alpha(r)\rangle_0(\pi r_0^2), \quad (28)$$

from which we would expect $\langle\sigma_{\rm SE}v\rangle$ to vary as $1/\sqrt{T}$ and κ_0 to be essentially temperature independent, as is confirmed by the large value of T_0 in (3). Since the measured value of $\langle\kappa_0\rangle \approx 5$, the phase difference $\phi_0 \approx 10^{-5}$, so that expressions (23) and (24), which are first order in ϕ_l, are essentially exact.

C. Estimate of $\langle\sigma_{\rm SE}v\rangle$

We will first briefly demonstrate the connection between the fully quantum-mechanical expressions (23) and (24) and the semiclassical expressions derived by Walker [14]. Then we will estimate a value for $\langle\sigma_{\rm SE}v\rangle$ given our measured value of κ_0 and the results of the semiclassical calculation.

The difference in the phase shifts can also be evaluated in the WKB approximation as [35, 36]

$$\phi_l = \frac{-m}{\hbar^2}\int_{r_c}^\infty \alpha(r)\left(k^2 - \frac{l(l+1)}{r^2} - \frac{2m}{\hbar^2}V_0(r)\right)^{-1/2} dr, \quad (29)$$

where r_c is the classical turning point. Using (29) rather than (22), and replacing the sum over angular momenta l by an integral over impact parameter, Eq. (23) reduces to the expression used by Walker. To calculate κ_0, Walker used a simpler expression due to Schaefer *et al.* [12]. The semiclassical approximation should be especially good for

the heavier noble gases, where many partial waves contribute to the scattering. In the case of helium, one can estimate from the interatomic potential [37, 38] that partial waves up to about $l \approx 16$ will contribute at room temperature.

Numerical evaluation of (23) and (24) to find $\langle\sigma_{SE}v\rangle$ and $\langle\kappa_0\rangle$ requires the matrix elements $\langle\alpha(r)\rangle_l$ between the radial eigenfunctions of the Hamiltonian (14). Evaluation of these matrix elements in turn requires the interatomic potential $V_0(r)$ and the function $\alpha(r)$. Since tabulated functions exist for both the interatomic potential [37, 38] and the Rb valence-electron wave function $\phi(r)$ [14, 39], the largest uncertainty comes from the wave-function enhancement factor η (12). As discussed earlier, the theoretical estimates for η differ by almost a factor of 2. However, the ratio

$$\beta \equiv \frac{\langle\sigma_{SE}v\rangle}{\langle\kappa_0\rangle^2} \tag{30}$$

is completely independent of η (to the extent that η is independent of r [12, 15]). The value for β then depends only on $V_0(r)$ and the unperturbed Rb valence-electron wave function $\phi(r)$. Furthermore, in the crude approximation of (27) and (28), we find that even the dependence on $\phi(r)$ drops out. Therefore we would expect the dominant uncertainty in β to stem from uncertainties in the interatomic potential.

Rather than numerically evaluate (23) and (24) we have chosen to use Walker's semiclassical estimate to find a value for β. We find $\beta = 4.5 \times 10^3$ Å^3/sec at 100 °C for the Rb-^{3}He system. The error on β will depend on the accuracy of the calculated interatomic potential of Ref. [37] and on the validity of the semiclassical approximation. Based on a comparison of the interatomic potentials of Refs. [37] and [38] and on Eqs. (27) and (28), we would expect the error in β to be about 20%. While it is difficult to reliably estimate the error on β since it depends on the accuracy of the calculated interatomic potential of Ref. [37] and on the validity of the semiclassical approximation, we guess that the error is probably less than 20%. Further quantum-mechanical calculations of β using (23) and (24) would be useful to determine its exact value and its uncertainty. In Table II we estimate the spin-exchange cross section using β and our measured value of $\kappa_0(T)$. Note that our estimate of $\langle\sigma v\rangle$ in Table II does not include any error in β.

TABLE II. Summary of values for $\langle\sigma_{SE}v\rangle$ for Rb–^{3}He at 100 °C. The experimental measurements of Refs. [2, 5, 16, 17] are scaled according to $1/\sqrt{T}$ assuming temperatures of 62, 190, and 165 °C, respectively. (We have estimated these temperatures to be those for which the major contribution to the cross section was made.) The error in the value quoted for the present work does *not* include any uncertainty in β (30) as calculated from the values in Ref. [14]. If the recent potential of Ref. [38] had been used in the calculation of β, rather than the potential of Ref. [37], one would expect a value for β that is 15% higher based on Eqs. (27) and (28). This adjusted value for β would give $\langle\sigma_{SE}v\rangle = 1.4 \times 10^{-19}$ cm^3/sec.

Reference	Method	$\langle\sigma_{SE}v\rangle$ (10^{-19} cm^3/sec)
Gamblin and Carver [2]	Expt.	1.77
Chupp *et al.* [5, 16]	Expt.	1.34 ± 0.22
Walker [14]	Theory	0.34–3.47
Larson *et al.* [17]	Expt.	0.66 ± 0.02
Present work	Calc. and expt.	1.2 ± 0.2

IV. DISCUSSION

A weighted average of the two absolute measurements of κ_0 combined with the measured temperature dependence gives

$$\kappa_0(100\,°\text{C}) = 5.17 \pm 0.37. \tag{31}$$

This value falls within the range of Walker's calculation of $\kappa_0 = 2.7-8.8$, confirming Walker, Bonin, and Happer's estimate of η [15].

The second intrinsic parameter describing the Rb-^{3}He system is the velocity-averaged cross section $\langle\sigma_{SE}v\rangle$. A value for this quantity is important for the understanding and design of polarized ^{3}He targets. The present values for $\langle\sigma_{SE}v\rangle$ in the literature differ by a factor of 2 (see Table II) [2, 5, 16, 17]. In the two most recent measurements, the nuclear relaxation rate of a polarized ^{3}He cell was measured at high temperatures and correspondingly at high Rb number density [Rb]. After correcting for any wall relaxation, the spin-relaxation time will be $\langle\sigma_{SE}v\rangle$[Rb]. Therefore, provided one can calculate [Rb] from the temperature T, the spin-relaxation time gives a value for $\langle\sigma_{SE}v\rangle$. Unfortunately, the vapor pressure depends exponentially on T [40] and this strong dependence makes any determination of the temperature dependence of $\langle\sigma_{SE}v\rangle$ difficult. Accordingly, the cross section is taken to be temperature independent in the analyses of these experiments. Uncertainties in the cell temperature, as well as in the relation between the vapor pressure and temperature, can lead to large errors in [Rb]. In addition, [Rb] is not solely determined by the temperature; chemical effects with the glass-cell walls may suppress [Rb]. As discussed in Sec. III, we can estimate a value for $\langle\sigma_{SE}v\rangle$ from Walker's calculations and from our measured value of κ_0 (see Table II). Our value for κ_0 predicts a value for $\langle\sigma_{SE}v\rangle$ from Eq. (30) of $(1.2\pm0.2)\times10^{-19}$ cm^3/sec, where the error does not include any uncertainty in β. Further numerical evaluation of β may allow a much more reliable estimate of $\langle\sigma_{SE}v\rangle$ from κ_0 than is possible with the more conventional methods.

The frequency shift (1) can be convienent for polarimetry of polarized ^{3}He targets. In previous polarized target work, the ^{3}He polarization P_{He} was determined by comparing ^{3}He AFP signals to water AFP signals as discussed in Sec. II B. Typically, the cells are held at room temperature and 30 G (a convenient field obtainable by 80-cm-diam Helmholtz coils of a modest-sized conductor). Depending on the size of the water cell and control of microphonics, the resulting AFP water signal can have a very poor signal-to noise ratio and limit the accuracy of P_{He}. Whereas frequency-shift polarimetry requires slightly more instrumentation, it has several ad-

vantages over the AFP. First, the frequency shift is intrinsic to the Rb-He system. Unlike the AFP technique of polarimetry, this new technique is not subject to drifts in the Q or the gain of the pick-up circuit. Furthermore, the shift in the EPR line for a 10-atm cell with $P_{\mathrm{He}} = 50\%$ is about 26 kHz. Using standard magnetometry techniques the EPR frequency shift can be measured to better than 1% of itself, so that the error in the ^{3}He polarization is dominated by the error in κ_0. We have presented a measurement of κ_0 accurate to about 8%. However, a new measurement in preparation using nonspherical geometries will improve this accuracy to the 2–3% level. The frequency-shift measurement can be made at fields of $\sim$1 G or less. This was an advantage in the experiment of Ref. [6]. Finally, with the use of a diode laser, the frequency-shift technique might be a much more local probe of the noble-gas polarization than the AFP technique. Provided care is taken to account for the weak-temperature dependence of κ_0 and the classical long-range frequency shift in nonspherical cells, frequency-shift polarimetry provides a nice alternative to NMR polarimetry.

We are currently pursuing more precise measurements of κ_0 in which we take advantage of the long-range classical frequency shift to calibrate the ^{3}He polarization. As discussed in the Introduction, this long-range shift can be a significant fraction of the total Rb EPR shift. With this new method of determining the ^{3}He polarization, the frequency-shift method of polarimetry becomes effectively self-calibrating.

ACKNOWLEDGMENTS

We gratefully acknowledge many helpful and encouraging discussions with Will Happer and Thad Walker. This research was supported by Air Force Office of Scientific Research Grants No. 88-0165 and No. F49620-92-J-0211.

[1] M. A. Bouchiat, T. R. Carver, and C. M. Varnum, Phys. Rev. Lett. **5**, 373 (1960).
[2] R. L. Gamblin and T. R. Carver, Phys. Rev. **138**, A946 (1965).
[3] W. Happer, E. Miron, S. Schaefer, D. Schreiber, W. A. van Wijngaarden, and X. Zeng, Phys. Rev. A **29**, 3092 (1984).
[4] X. Zeng, Z. Wu, T. Call, E. Miron, D. Schreiber, and W. Happer, Phys. Rev. A **31**, 260 (1985).
[5] T. E. Chupp, M. E. Wagshul, K. P. Coulter, A. B. McDonald, and W. Happer, Phys. Rev. C **36**, 2244 (1987).
[6] N. R. Newbury *et al.*, Phys. Rev. Lett. **67**, 3219 (1991); **69**, 391 (1992).
[7] T. E. Chupp and R. J. Hoare, Phys. Rev. Lett. **64**, 2261 (1990); T. E. Chupp *et al.*, *ibid.* **63**, 1541 (1989).
[8] A. K. Thompson *et al.*, Phys. Rev. Lett. **68**, 2901 (1992).
[9] B. Larson *et al.*, Phys. Rev. Lett. **67**, 3356 (1991).
[10] K. P. Coulter *et al.*, Nucl. Instrum. Methods Phys. Res. A **288**, 463 (1990).
[11] R. Arnold *et al.*, Proposal to SLAC Experimental Program Advisory Committee No. E-142 (1989) (unpublished).
[12] S. R. Schaefer, G. D. Cates, Ting-Ray Chien, D. Gonatas, W. Happer, and T. G. Walker, Phys. Rev. A **39**, 5613 (1989).
[13] B. C. Grover, Phys. Rev. Lett. **40**, 391 (1978).
[14] T. G. Walker, Phys. Rev. A **40**, 4959 (1989).
[15] T. G. Walker, K. Bonin, and W. Happer, Phys. Rev. A **35**, 3749 (1987).
[16] K. P. Coulter, A. B. McDonald, W. Happer, T. E. Chupp, and M. E. Wagshul, Nucl. Instrum. Methods Phys. Res. A **270**, 90 (1988).
[17] B. Larson, O. Häusser, P. P. J. Delheij, D. M. Whittal, and D. Thiessen, Phys. Rev. A **44**, 3108 (1991).
[18] W. Happer and S. Svanberg, Phys. Rev. A **9**, 508 (1974).
[19] W. Happer and H. Tang, Phys. Rev. Lett. **31**, 273 (1973).
[20] L. C. Balling, R. J. Hanson, and F. M. Pipkin, Phys. Rev. **133**, A607 (1964); L. C. Balling and F. M. Pipkin, *ibid.* **136**, A46 (1964).
[21] F. Bloch and A. Siegert, Phys. Rev. **57**, 522 (1940).
[22] G. D. Cates, S. R. Schaefer, and W. Happer, Phys. Rev. A **37**, 2877 (1988).
[23] N. R. Newbury, Ph.D. thesis, Princeton University, 1992 (unpublished).
[24] M. Kitano *et al.*, Phys. Rev. C **34**, 1974 (1986).
[25] W. Farr and E.-W. Otten, Appl. Phys. **3**, 367 (1974).
[26] A. L. Bloom, Appl. Opt. **1**, 61 (1962); W. E. Bell and A. L. Bloom, Phys. Rev. **107**, 1559 (1957).
[27] A. Abragam, *Principles of Nuclear Magnetism* (Oxford University Press, Oxford, 1961); E. R. Andrews, *Nuclear Magnetic Resonance* (Cambridge University Press, Cambridge, 1958).
[28] K. P. Coulter, Ph.D. thesis, Princeton University, 1989 (unpublished).
[29] W. Happer, Rev. Mod. Phys. **44**, 160 (1972).
[30] R. M. Herman, Phys. Rev. **137**, A1062 (1965).
[31] A. Dalgarno, Proc. R. Soc. London Ser. A **262**, 132 (1961).
[32] A. E. Glassgold, Phys. Rev. **132**, 2144 (1963).
[33] P. L. Bender, Phys. Rev. **134**, A1174 (1964).
[34] C. K. Chang and R. H. Walker, Phys. Rev. **178**, 198 (1969).
[35] Albert Messiah, *Quantum Mechanics* (Wiley, New York, 1976), Vol. 1, pp. 405–410.
[36] L. S. Rodberg and R. M. Thaler, *Introduction to the Quantum Theory of Scattering* (Academic, New York, 1967).
[37] J. Pascale, Phys. Rev. A **28**, 632 (1983).
[38] K. E. Gibble and J. Cooper, Phys. Rev. A **44**, R5335 (1991).
[39] D. R. Bates and A. Damgaard, Philos. Trans. R. Soc. London **242**, 101 (1949); M. J. Seaton, Mon. Not. R. Astron. Soc. **188**, 504 (1969).
[40] T. J. Killian, Phys. Rev. **27**, 578 (1926).